Journal of Materials Processing Technology 150 (2004) 242–254

Journal of Materials Processing Technology

www.elsevier.com/locate/jmatprotec

Bending behaviour of corrugated web beams

Y.A. Khalid*, C.L. Chan, B.B. Sahari, A.M.S. Hamouda

Department of Mechanical and Manufacturing Engineering, University Putra Malaysia, Serdang, 43400 Selangor, Malaysia

Received 18 June 2003; accepted 3 February 2004

Abstract

The paper is devoted to the behaviour of mild steel structural beams with corrugated web subjected to three-point bending. Semicircular web corrugation in the cross-sectional plane (horizontal) and across the span of the beam (vertical) were investigated both experimental and computationally using finite element technique. In the finite element analysis, test specimen was modelled using commercially available finite element software LUSAS and a non-linear analysis was performed. Corrugation radius of 22.5 and 4 mm thickness, with constant corrugation amplitude to cycle length ratio (H/λ) and flange thickness of 6 mm were selected as the base sizes. The plane web beams, welded and ordinary rolled, were also tested with both methods to develop the benchmark results. The comparisons between the experimental and the finite element analysis results were satisfactory. It was noted that the vertical-corrugated web beam (VCRx) could carry between 13.3 and 32.8% higher moment comparing to the plane and horizontal-corrugated web beams, for the range of corrugation radius taken. Besides that, larger corrugation radius could sustain higher bending load up to the yielding stage. This attributed to the increment of the second moment of area (I) that has influence on the direct bending stresses (σ_{zz}). In addition, reduction in weight could be achieved by using the vertical-corrugated web. This is true for the corrugation shapes and sizes taken throughout this study.

Keywords: Semicircular corrugated web; Bending strength; Corrugation direction; Corrugation radius; Cross-sectional area; Weight reduction

1. Introduction

The I-section beams or H-piles are commonly used in structural steel works. Ordinary shapes of these beams are constructed from two parallel flanges and a web where about 30–40% of the entire weight of a medium flange width or narrow flange type of beam is contributed by the web part.

In construction application, the web usually bears most of the compressive stress and transmits shear in the beam while the flanges support the major external loads. Thus, by using greater part of the material for the flanges and thinner web, materials saving could be achieved without weakening the load-carrying capability of the beam [1]. Nevertheless, as the compressive stress in the web has exceeded the critical point prior to the occurrence of yielding, the flat web loses its stability and deforms transversely. This could be improved by using corrugated web, an alternative to the plane web, which produces higher stability and strength without additional stiffening and use of larger thickness.

The early studies on the corrugated web were concentrated on the vertically trapezoidal corrugation. Elgaaly investigated the failure mechanisms of these beams under different loading modes, namely shear mode [2], bending mode [3] and compressive patch loads [4]. They found that the web could be neglected in the beam bending design calculation due to its insignificant contribution to the beam's load-carrying capability. Besides that, the two distinct modes of failure under the effect of patch loading were dependent on the loading position and the corrugation parameters. These are found agreeable to the investigation by Johnson and Cafolla and were further discussed in their writings [5,6]. In addition, the experimental tests conducted by Li et al. [7] showed that the corrugated web beam has 1.5–2 times higher buckling resistance than the plane web type.

This paper describes the investigation carried out on the bending behaviour of mild steel beams with semicircular web corrugation. The aim of this study is to determine the effects of corrugated web and the corrugation direction to the beam's load-carrying capability. Experimental tests and finite element method were adopted for these purposes. Two corrugation directions, in the cross-sectional plane (horizontal) and across the beam span (vertical), were considered while the ordinary plane web beams were also tested to develop the benchmark results. The effect of the corrugation radius, web thickness and material properties for the vertical-corrugated web beam type were investigated. The

* Corresponding author. Tel.: +60-3-89486101x2082; fax: +60-3-89488939.
E-mail address: yousif@eng.upm.edu.my (Y.A. Khalid).

0924-0136/$ – see front matter © 2004 Elsevier B.V. All rights reserved.
doi:10.1016/j.jmatprotec.2004.02.042

Nomenclature

A_{xy}	area of cross-section in the *xy*-plane
A_{zx}	area of cross-section in the *zx*-plane
b_f	width of flange
d	depth of beam
$d_m = 2r_m$	mean diameter of corrugated web
E	modulus of elasticity
F_U	ultimate load
F_y	yield load
I_{xx}	second moment of area with respect to the *x*-axis
L	length of beam
M_U	maximum bending moment
M_y	yield bending moment
p	loading position on vertically corrugated web beam
r	corrugation radius ($r = r_m$ in this work)
r_i	inner radius/minor radius of corrugated web
r_o	outer radius/major radius of corrugated web
S	elastic section modulus
t	web thickness at cross-section
t_f	flange thickness
t_w	web thickness
V	volume
w	weight per unit length
W	specific weight
σ_{zz}	bending stress in the *z*-axis

experimental results were also compared with the computational results.

2. Experimental tests

2.1. Test specimens

Five models of beams were selected for the experimental tests and designated as: OPW, WPW1, HC1R1-1, HC2R1-1 and VCR3-1. The detail dimensions of these test specimens are given in Table 1 and illustrated in Fig. 1. The two parallel flanges were made from flat bar of 75 mm wide and 6 mm thick, while strip and pipe of an outer diameter of 49 and 4 mm thickness were used to produce both the plane and the corrugated shapes of the web. The pipes were split equally by using milling machine and joint-welded to form the corrugation shape in both horizontal and vertical directions. The consumable electrode of 2.6 mm diameter and 300 mm long (AWS E6013) was used throughout the process of welding. It should be emphasised that only one layer of arc welding was done on all specimens, which is sufficient for static loading and in mean-time reduces the influence of welding to the specimen's behaviour. All the beams tested were 600 mm in length. The wide-flange beam (OPW) of 77 mm flange width and 127 mm deep was selected to be the base for this investigation.

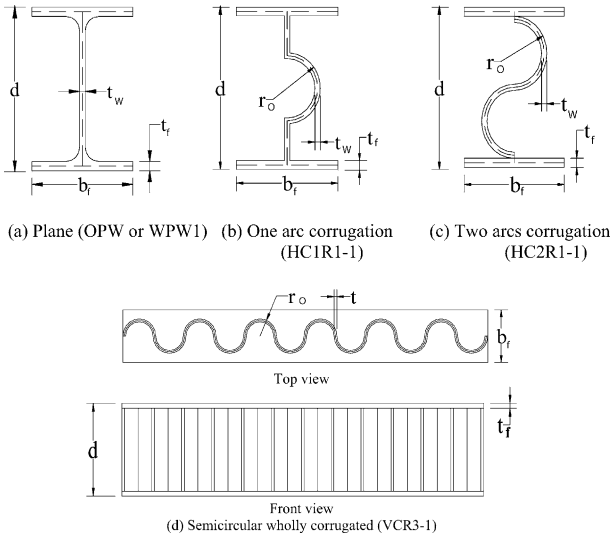

(a) Plane (OPW or WPW1) (b) One arc corrugation (HC1R1-1) (c) Two arcs corrugation (HC2R1-1)

(d) Semicircular wholly corrugated (VCR3-1)

Fig. 1. Geometry of the models tested experimentally.

In addition, coupons were also collected from the ordinary I-section beams (at top, bottom flanges and the web) and were tested for its material properties. The size of the tensile specimens fabricated was referred to the standard test methods and definitions for mechanical testing of steel products from the American Society for Testing and Materials (ASTM). Similar tests were also done on the flat bars and pipes.

Table 1
Test specimens' dimensions

Type	Designation	d (mm)	t_f (mm)	b_f (mm)	t_w/t	R_o (mm)
Plane						
Rolled	OPW	127.05	7.05	77.00	4.45	–
Welded	WPW1	113.60	6.00	75.00	4.50	–
Horizontal-corrugated						
One arc	HC1R1-1	111.80	6.00	75.00	4.00	24.50
Two arcs	HC2R1-1	106.00	6.00	75.00	4.00	24.50
Vertical-corrugated						
Semicircular wholly corrugated	VCR3-1	106.00	6.00	75.00	4.00	24.50

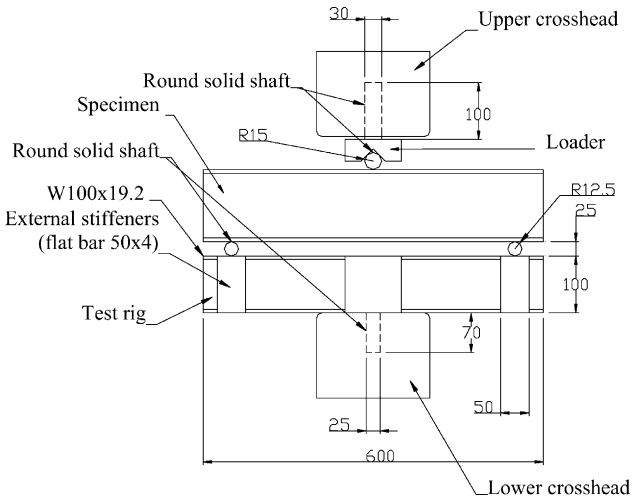

Fig. 2. Detail dimensions of experiment test rig (in mm).

2.2. Test set-up

A test rig was designed and commissioned as the base support for the test specimens and in providing the three-point bending condition as shown in Fig. 2. All parts are welded in multiple layers so that the rig is rigid and undistorted under the action of loading. This rig was fitted and gripped in the lower cross-head of the universal testing machine (Instron Model 8500 Plus), which has the maximum load capacity of 250 kN and able to perform various loading modes. The specimens were rested on the solid shafts of the rig and the load was applied across the width of the top flange at an equal distance from both supported points. For the vertical-corrugated web specimens (VCR3), the load was applied at the joint between the two semicircles, which has the largest cross-sectional area. The span length was kept as 500 mm for all the test specimens.

Three tests were carried out for each beam type where the automatic displacement control mode was implemented in order to obtain uniform deformation. The cross-head speed was set at 3.0 mm/min throughout these tests. This moderate loading speed could reduce the load fluctuation due to the hydraulic powered loading principle and prevent the occurrence of abrupt failure. As for the tensile tests, the standard cross-head speed of 2.54 mm/min was implemented.

3. Test results and discussion

The average values of yield stress and ultimate strength obtained from the tensile tests for ordinary I-section beam (M1), flat bar (M2) and pipe (M3) are given in Table 2. The load-machine cross-head displacement curves, for each beam model tested under three-point bending, are shown in Figs. 3 and 4. The yield and ultimate points were determined from these graphs and the average load and moment values were calculated, as given in Table 3. It was found that the vertical-corrugated web beams (VCR3-1) could sustain more loads up to the yielding and ultimate state when compared to other types of beam tested. The lowest ratios obtained when compared with the horizontal-corrugated web beam type (HC1R1-1 and HC2R1-1) were as much as 1.79 and 1.91 times higher. This is mainly attributed to the greater resistance against the buckling deformation of the compressive flange vertically into the corrugated web and larger second moment of area, I_{xx}. On the other hand, the OPW specimens has the highest values for both yield and ultimate loads mainly due to the fabrication method and flange's material and geometry differences, which have not been addressed in this study. Besides that, the welded plane web (WPW1), specimens showed lower yield load but higher ultimate value than VCR3-1 specimens at about 7.47 and 18.96%, respectively, which was contributed by the

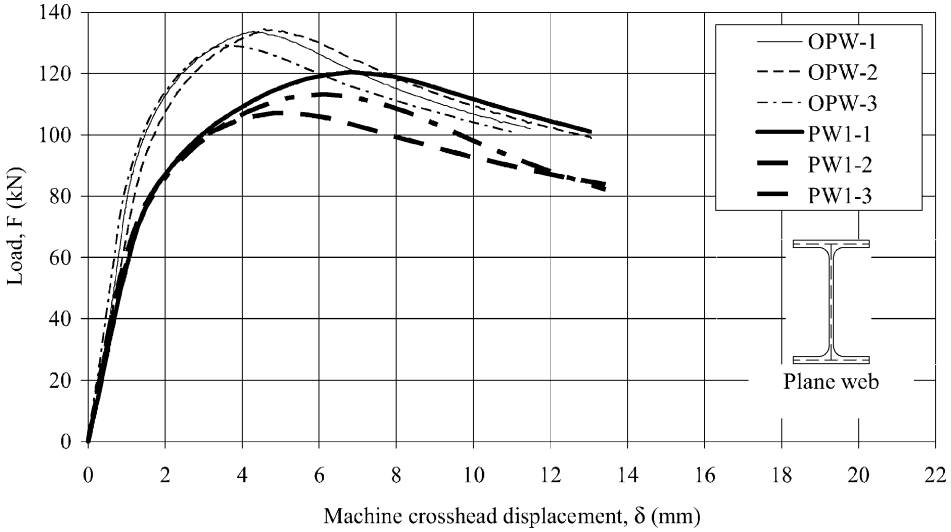

Fig. 3. F–δ curves (plane web beams).

Table 2
Tensile test results

Material	Designation	E (kN mm^{-2})	σ_y (N mm^{-2})	σ_U (N mm^{-2})
I-section or W-shape beam	M1	200	355	473
Flat bar	M2	200	346.4	446.4
Pipe	M3	200	322	362

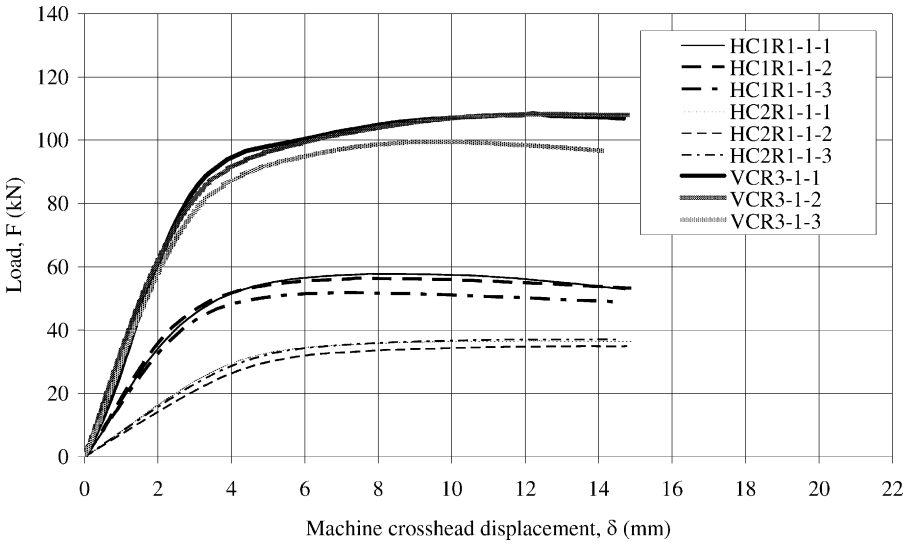

Fig. 4. F–δ curves (corrugated web beams).

influence of the position of supports. The specimens were supported at the weaker point on a cycle of corrugation and thus; failure progressed rapidly beyond the yield point of the bottom flange. Throughout these tests, it was also observed that the specimens gradually bend till the compression flange yielded and subsequently buckled vertically into the crippled web. Though, the web crippling failure was not significantly seen from the HC2R1-1 and VCR3-1 specimens. Samples of the different models at failure are shown in Fig. 5.

On the other hand, the I-beams show bending of the flanges first, which has been followed by web rippling. Moreover, the horizontal-corrugated web type of beams show a flange bending first, then compressed at the adjoining arcs of the web which causes the arcs opening to

Table 3
Experimental yield and ultimate values

Type	Test	Yield load, F_y (kN)	Average	Yield moment, M_y (MN mm)	Ultimate load, F_U (kN)	Average	Ultimate moment, M_U (MN mm)
OPW	1	79.813	75.603	37.802	134.118	132.116	66.058
	2	75.613			133.000		
	3	71.384			129.231		
WPW1	1	61.222	54.791	27.396	120.513	113.505	56.753
	2	46.242			106.957		
	3	56.910			113.044		
HC1R1-1	1	37.239	37.793	18.897	57.750	55.337	27.669
	2	37.371			56.522		
	3	38.770			51.739		
HC2R1-1	1	28.582	30.157	15.079	36.912	36.352	18.176
	2	29.892			35.000		
	3	31.997			37.143		
VCR3-1	1	71.797	67.608	33.804	108.421	105.614	52.807
	2	60.840			108.421		
	3	70.188			100.000		

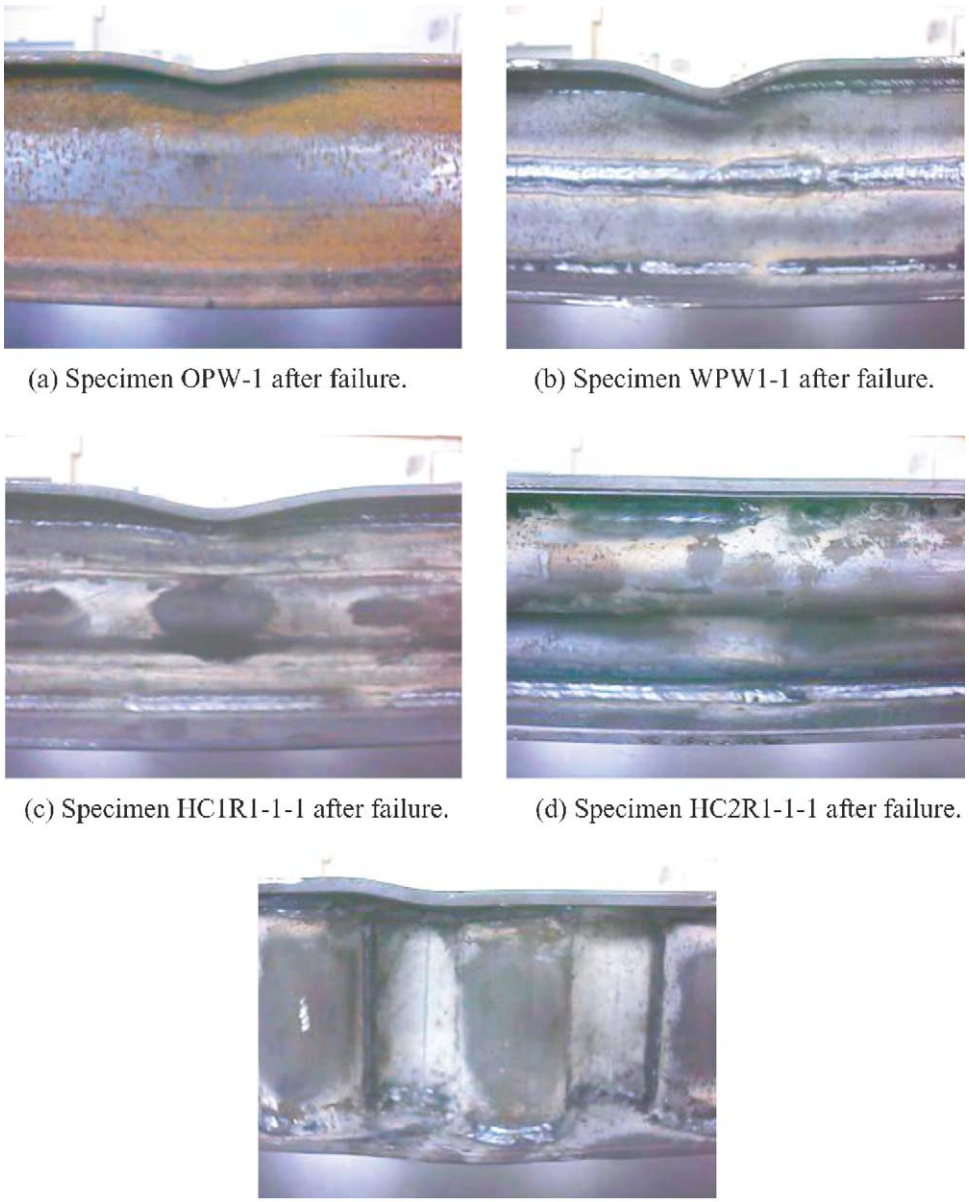

(a) Specimen OPW-1 after failure.

(b) Specimen WPW1-1 after failure.

(c) Specimen HC1R1-1-1 after failure.

(d) Specimen HC2R1-1-1 after failure.

(e) Specimen VCR3-1-1 after failure.

Fig. 5. Experimental test specimens at failure.

close. Furthermore, the vertical web type of beams, show also a flange bending at the first stage, then no web rippling appears to occur.

Even though, the welded test specimens were done carefully, still some imperfections as the small initial bending of the flanges from the intense heat generated by welding occur. The deformation appears to be negligible and no weld failure occurred throughout these tests.

4. Finite element modelling

The five types of beam tested in the experimental part were modelled with quadrilateral thick shell elements (QTS8) and analysed by using LUSAS software package. By utilizing the geometry-symmetrical behaviour in the *xy*-plane, half span models were created for the plane web and horizontal-corrugated web beams while full models for the vertical-corrugated web type were generated. The typical finite element models generated are shown in Fig. 6 and the geometry dimensions for each model are given in Table 4.

For the materials attributes, the elasto-plastic isotropic stress potential model was adopted throughout this study. It is a non-linear von Mises material model applicable to a general multi-axial stress state and supports three hardening definitions. The modulus of elasticity ($E = 200\,\mathrm{GN/m^2}$) and the Poisson ratio ($\nu = 0.3$) have been used as the elastic input data, while the other required material properties are

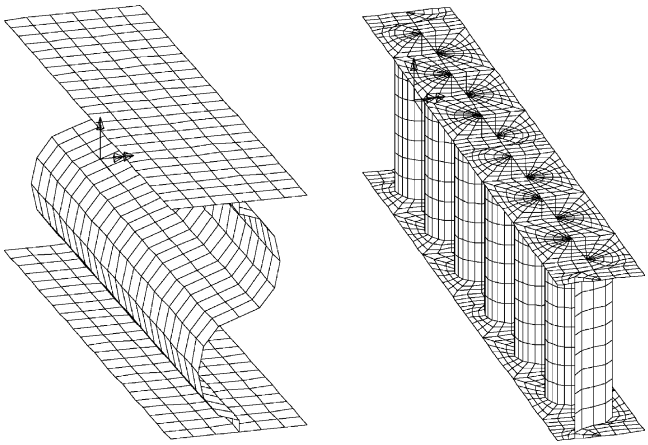

Fig. 6. Half span model (left) and full span model (right).

shown in Table 2. However, the geometric attributes were merely described by the surfaces' thickness, t (as given in Table 4). The input date, for each model generated are given in Table 5. Global distributed load was applied to the line feature along the centreline of the beam span at an equal distance from both the supported ends. It should be emphasised that the load was applied in the same direction as occurred in the experimental tests where during loading the movement was governed by the machine's jacks in a single direction. The simulation of loading is shown in Fig. 7.

5. Results and discussion

A total of 30 finite element models were created and tested using LUSAS software package. All models were assigned with different geometry and material properties to explore the influences of each variable to the beam's moment carrying capacity (refer Tables 4 and 5). Load–displacement graphs were plotted for each case as shown in Figs. 8–11. All the welded I-beam tests are collected in Fig. 8. The effect of the web and flange material could be observed from the comparison between group specimen nos. 2–4 to specimen nos. 4–6.

Table 4
Analytical models dimensions

Type	Designation	d (mm)	t_f (mm)	b_f (mm)	t_w/t	R_o (mm)	L (mm)
Plane							
Rolled	OPW	127.05	7.05	77.00	4.45	–	500.00
Welded (WPW*x*)	WPW1	113.60	6.00	75.00	4.50	–	500.00
	WPW2	113.60	6.00	75.00	4.00	–	500.00
	WPW3	113.60	6.00	75.00	4.00	–	500.00
	WPW4	113.60	6.00	75.00	4.00	–	500.00
	WPW5	106.00	6.00	75.00	4.00	–	500.00
	WPW6	106.00	6.00	75.00	4.00	–	540.00
Horizontally corrugated							
One arc (HC1R*x*)	HC1R1-1	111.80	6.00	75.00	4.00	24.50	500.00
	HC1R1-2	111.80	6.00	75.00	4.00	24.50	500.00
	HC1R1-3	106.00	6.00	75.00	4.00	24.50	500.00
	HC1R1-4	106.00	6.00	75.00	4.00	24.50	540.00
	HC1R2-1	111.80	6.00	75.00	4.00	35.75	500.00
	HC1R2-2	111.80	6.00	75.00	4.00	35.75	500.00
	HC1R2-3	106.00	6.00	75.00	4.00	35.75	540.00
	HC1R3-1	111.80	6.00	75.00	4.00	69.50	500.00
	HC1R3-2	111.80	6.00	75.00	4.00	69.50	500.00
	HC1R3-3	106.00	6.00	75.00	4.00	69.50	540.00
Two arcs (HC2R*x*)	HC2R1-1	106.00	6.00	75.00	4.00	24.50	500.00
	HC2R1-2	106.00	6.00	75.00	4.00	24.50	540.0
	HC2R2-1	106.00	6.00	75.00	4.00	35.75	500.00
	HC2R2-2	106.00	6.00	75.00	4.00	35.75	540.00
	HC2R3-1	106.00	6.00	75.00	4.00	69.50	500.00
	HC2R3-2	106.00	6.00	75.00	4.00	69.50	540.00
Vertically corrugated							
Semicircular wholly corrugated	VCR1	106.00	6.00	75.00	4.00	13.25	540.00
(VCR*x*) one arc (HC1R*x*)	VCR2	106.00	6.00	75.00	4.00	18.875	540.00
	VCR3-1	106.00	6.00	75.00	4.00	24.50	500.00
	VCR3-2	106.00	6.00	75.00	4.00	24.50	540.00
	VCR3-3	106.00	6.00	75.00	3.00	24.00	540.00
	VCR3-4	106.00	6.00	75.00	3.00	24.00	540.00
	VCR4	106.00	6.00	75.00	4.00	29.00	540.00
	VCR5	106.00	6.00	75.00	4.00	35.75	540.00

Table 5
Assignment of material attributes

Model	Material		
	Flange	Web	
		Flat section	Corrugated section
Plane			
OPW	M1	M1	–
WPW1/2	M2	M2	–
WPW3	M1	M1	–
WPW4/5/6	M2	M3	–
One arc horizontal-corrugated			
HC1R1-1	M2	M2	M3
HC1R1-2/3/4	M2	M3	M3
HC1R2-1	M2	M2	M3
HC1R2-2/3	M2	M3	M3
HC1R3-1	M2	M2	M3
HC1R3-2/3	M2	M3	M3
Two arcs horizontal-corrugated			
HC2R1-1/2	M2	–	M3
HC2R2-1/2	M2	–	M3
HC2R3-1/2	M2	–	M3
Semicircular wholly vertical-corrugated			
VCR1	M2	–	M3
VCR2	M2	–	M3
VCR3-1/2/3	M2	–	M3
VCR3-4	M2	–	M2
VCR4	M2	–	M3
VCR5	M2	–	M3

Specimen nos. 4–6 have the same web material (M3) and different flange materials of M1–M3. On the other hand, group specimen nos. 4–6 have the same flange material (M3) and different web materials of M1–M3. It could be seen from this comparison (Fig. 8) that the web material has a great effect on the moment carrying capacity. The increase of the moment carrying capacity has been found as 16.05% when the web material changed from M3 to M1. However, the increase in the moment carrying capacity is only 10.09% when M1 is used instead of M3 for the flanges. It is important to mention here that all the models were of the same dimensions and boundary conditions.

For the benefit of comparison, the author utilised the terms load to weight per unit length ratio (F_y/w) and elastic section modulus (S). The F_y is defined as the transition point of the load and displacement relationship, from the linear to the non-linear behaviour. The yield loads obtained from analyses and calculated values for the aforesaid variables were tabulated in Table 6. In addition, the $(M_y/w)/(M_y/w)_{WPW7}$ and S/S_{WPW7} ratios were also calculated for the finite element models with the same geometry dimensions and material properties and drawn as bar chart, shown in Fig. 12. The main purpose of doing this is to facilitate in evaluation of the real performance of each beam unaffected by any influential factors.

As shown in Table 6 and Fig. 12, the VCR beams could carry high load compared to the plane web beams (WPW) and horizontal-corrugated web beams (HC1R and

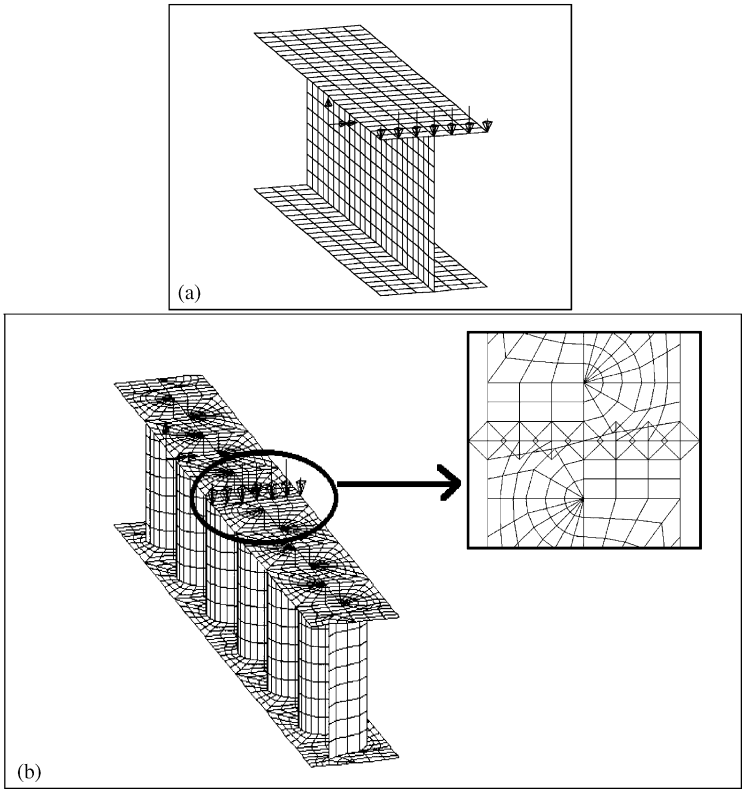

Fig. 7. Load simulation for (a) half model and (b) full model.

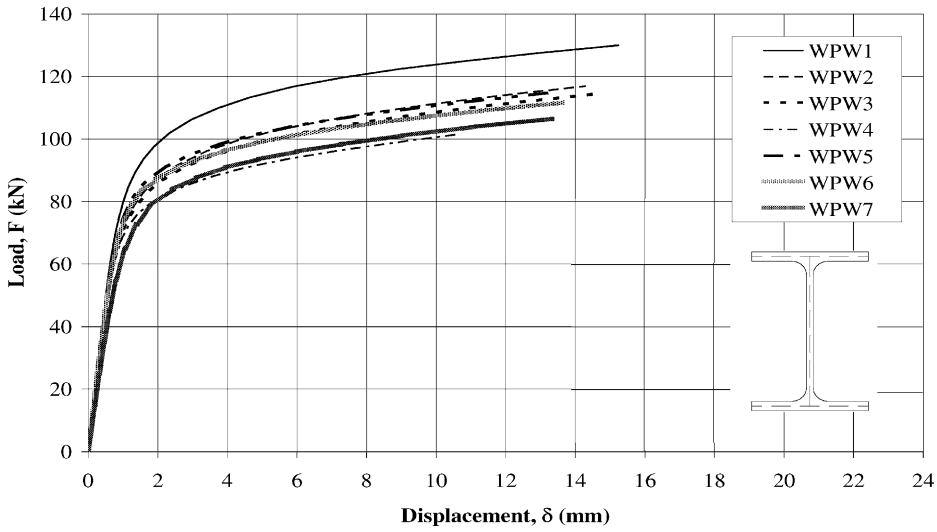

Fig. 8. *F–δ* curves (FEA plane web beams).

HC2R), up to the yielding stage. The *M*/*w* ratio obtained falls in the range of 0.970–1.136 for these cases. This is mainly attributed to the larger cross-sectional area that contributed about 15–34% increment in the *S* values which has significant influence on the load-carrying capability. Thus, a reduction in weight by as much as 13.6% is possible to be achieved by using the thinner material for the web with vertical-corrugation. On the other hand, for the horizontal-corrugated web type, the one arc corrugation profile (HC1R) could sustain higher values of moment than the two arcs profile (HC2R); in the range of 1.19–1.73 times. This is attributed to the construction of the HC2R beams which has higher tendency to be compressed under the action of concentrate load. Moreover, greater improvements in the beam's bending strength, specifically the VCR*x* beams, was achieved by using thicker and stronger material for the web part comparing to the negligible contribution brought by the change in both depth and length (as shown in VCR3 models). The stress distribution (σ_{zz}) at the loaded section for geometrically identical models with different web shape were shown in Fig. 13. In this figure, the effect of using the vertical-corrugated web could be observed, where the bending stress at the web part is negligible and most of the load appears to be carried out by the flanges, when compared to the other types of beams tested. On the other hand, HC2R1-2 model shows a high bending stress because its horizontal web has limited resistance to bending. This is mainly attributed to the deformation mode where the cap is closing for the top and bottom halves of this model. This will cause a high stress concentration at the quadrant points of both the arcs of this type of models.

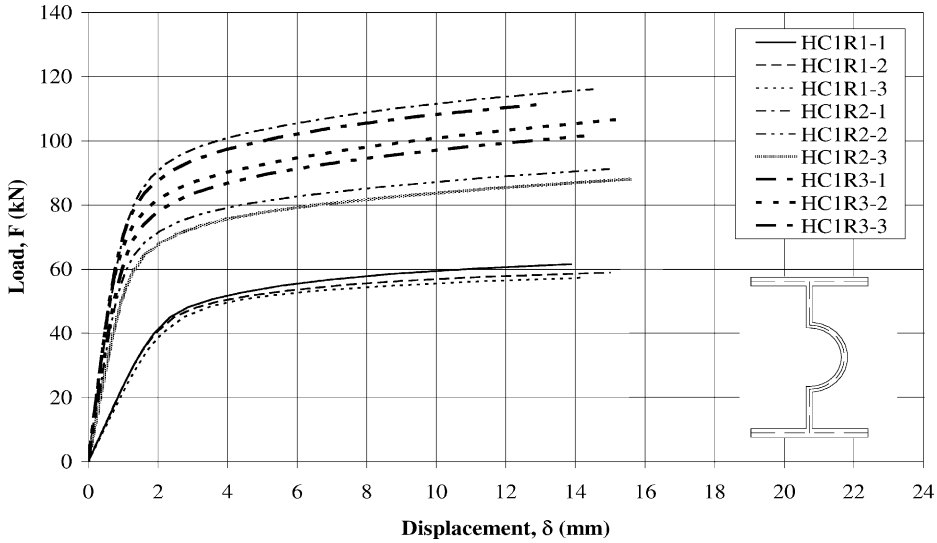

Fig. 9. *F–δ* curves (FEA horizontal-corrugated web beams HC1R*x*).

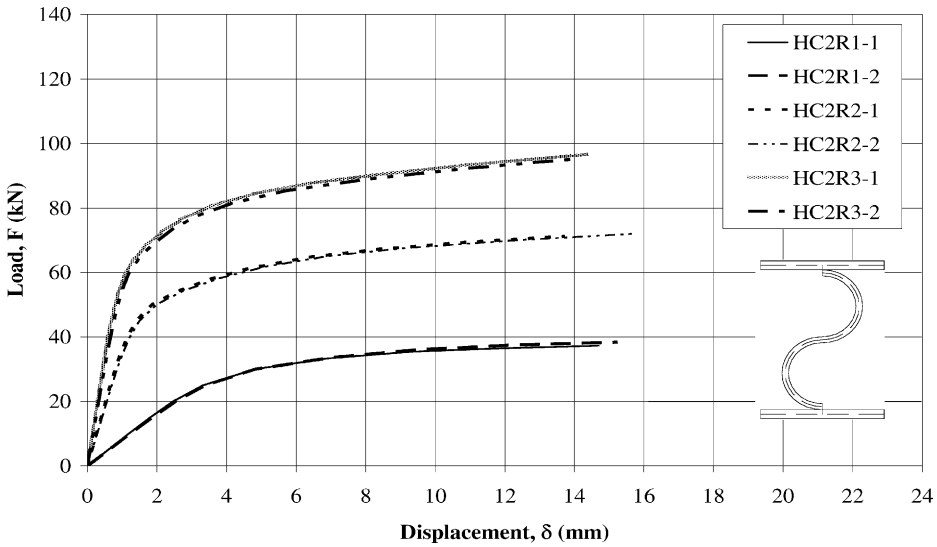

Fig. 10. *F–δ* curves (FEA horizontal-corrugated web beams HC12R*x*).

All the finite element models bend at the early stage, while the horizontal-corrugated web models show an arcs gap closing. Furthermore, no web rippling has been noticed for the vertical-corrugated models.

6. Correlation between corrugation radius, I_{xx} and bending moment

The cross-sectional area of the vertical-corrugated web beam was analysed to study the correlation between the bending moment (M), area moments of inertia (I_{xx}) and the corrugation radius ($r = r_m$). Throughout these analytical tests, three radius ratios of 1.0, 1.5 and 3.0 were taken for the horizontal-corrugated models while five radius ratios in the range of 0.5–1.5 for the vertical-corrugated models. It should be emphasised that the corrugation radius is measured in terms of the mean radius of a semicircle (r_m) and the radius ratio was taken as the multiply of 22.5 mm (experimental specimens' radius).

It was noted that the vertical-corrugated web beam has a varying cross-section area across its length while uniform for the others (see Fig. 1). Consequently, a multiple value of area moments of inertia is obtainable across the span. From the elastic bending equation ($\sigma_{zz} = M_y/I$), where the same value of bending stress is concerned, the moment is inversely proportional to the area moment of inertia.

Besides that, the yield load (F_y) is found to be correlated to the size of corrugation radius (r_m), where the F_y increases as the r_m increases. This trend was observed in both the horizontal and vertical-corrugated web models. Furthermore, the greater advancement was obtained from both the

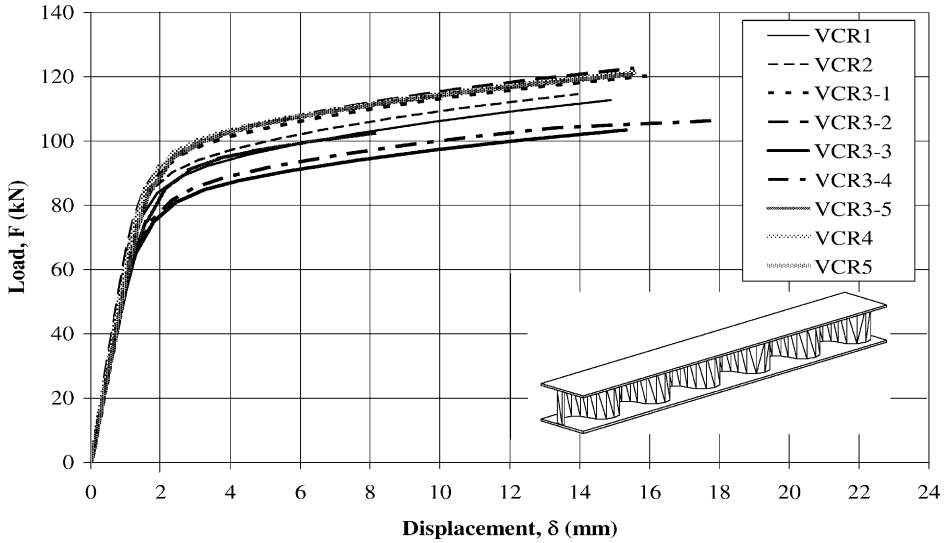

Fig. 11. *F–δ* curves (FEA vertical-corrugated web beams VCR*x*).

Table 6
Finite element analysis results

Model	F_y (kN)	Volume (V) (mm^3)	F_y/w (Nm kg^{-1})	I_{xx} (mm^4)	S (mm^3)
OPW	82.045	821634.14	6352.16	4450000.0	70051.16
WPW1	64.574	678600.00	6053.29	3000000.0	52816.90
WPW2	59.709	653200.00	5814.88	2957000.0	52059.86
WPW3	64.001	653200.00	6232.87	2957000.0	52059.86
WPW4	55.374	653200.00	5392.71	2957000.0	52059.86
WPW5	55.513	638000.00	5535.05	2529000.0	47716.98
WPW6	55.239	689040.00	5507.73	2529000.0	47716.98
HC1R1-1	35.043	693409.03	3214.84	2862564.0	51208.66
HC1R1-2	33.055	693409.03	3032.46	2862564.0	51208.66
HC1R1-3	33.162	681809.36	3094.03	2539519.0	47915.45
HC1R1-4	33.168	736354.11	3094.59	2539519.0	47915.45
HC1R2-1	56.703	655276.72	5504.64	2877674.0	51478.96
HC1R2-2	51.586	655276.72	5007.89	2877674.0	51478.96
HC1R2-3	46.891	695170.84	4634.14	2554629.0	48200.55
HC1R3-1	60.024	650203.70	5872.50	3032662.0	54251.56
HC1R3-2	55.424	650203.70	5422.45	3032662.0	54251.56
HC1R3-3	55.726	689691.99	5551.03	2709617.0	51124.85
HC2R1-1	21.601	732743.34	1875.29	2467974.0	46565.55
HC2R1-2	19.209	791362.81	1667.63	2467974.0	46565.55
HC2R2-1	37.914	646554.06	3730.29	2388370.0	45063.58
HC2R2-2	37.925	698178.38	3731.90	2388370.0	45063.58
HC2R3-1	46.845	659451.50	4518.85	2377060.0	44850.19
HC2R3-2	46.899	712207.62	4524.06	2377060.0	44850.19
VCR1	62.601	804934.34	5343.08	2909334.3	54893.10
VCR2	63.292	804934.30	5402.06	3056909.5	57677.54
VCR3-1	72.709	744240.48	6214.73	3181321.3	60024.93
VCR3-2	73.078	804934.25	6237.31	3181321.3	60024.93
VCR3-3	53.998	725200.65	5115.53	3170945.2	59829.15
VCR3-4	63.304	725200.65	5997.14	3170945.2	59829.15
VCR4	73.178	804934.20	6245.85	3269953.6	61697.24
VCR5	73.328	804934.16	6258.65	3390024.2	63962.72

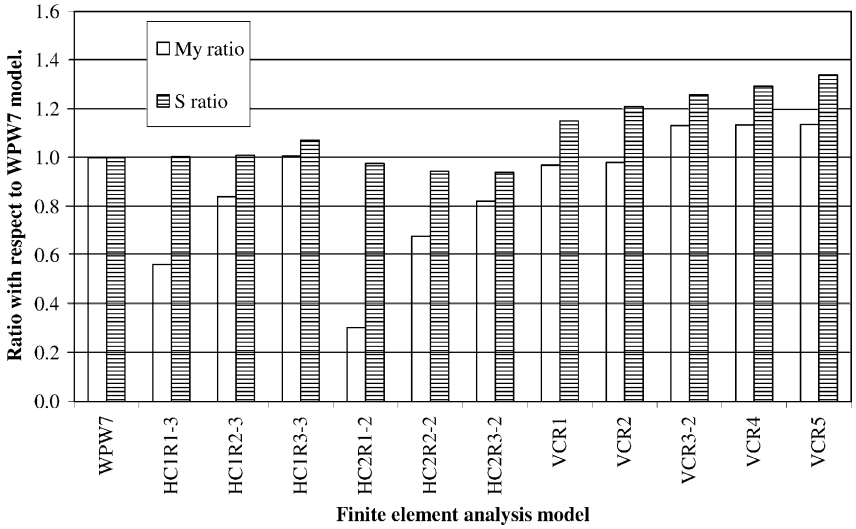

Fig. 12. M_y and S ratio with respect to WPW7 model.

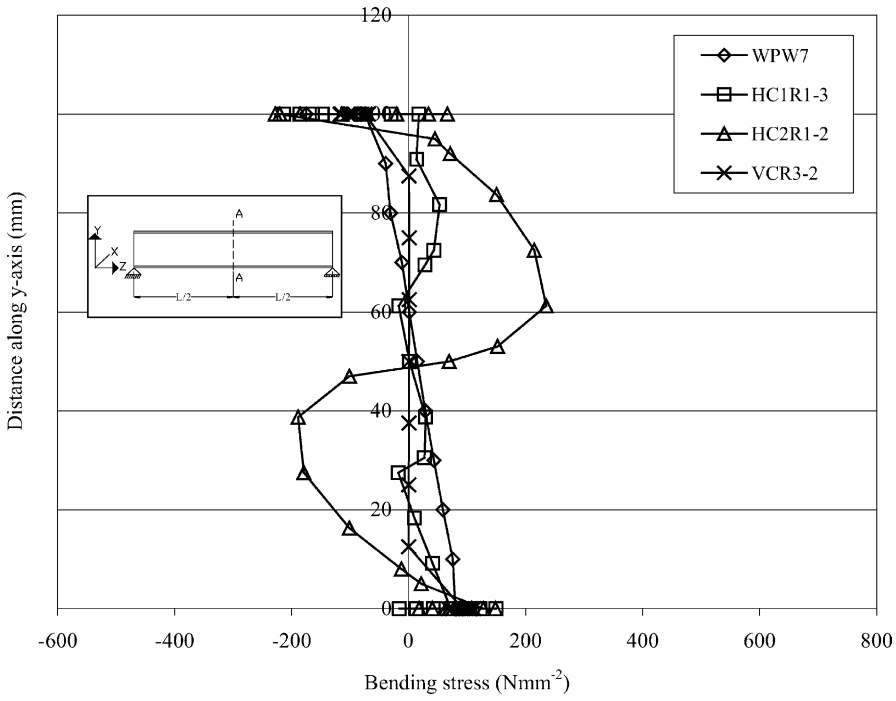

Fig. 13. Bending stress distribution at section A-A on geometrically identical finite element models with different web shape (at 35 kN load).

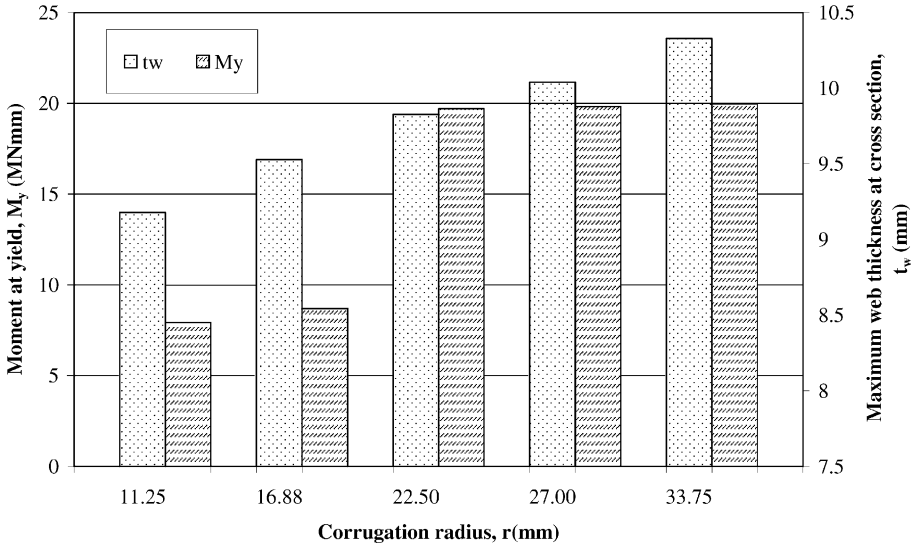

Fig. 14. Correlation between M_y, t_w and r.

HC1R1 and HC2R2 models compared with the VCR*x*, at about 68, 144 and 17%, respectively. The correlations between the moment at yield (M_y), elastic section modulus (S), web thickness (t_w) and corrugation radius (r measured as r_m) are shown in Fig. 14.

7. Results comparison

From the comparison between the experimental and finite element analysis results, the percentage of difference obtained were in the range of 7.28–28.37%. This is mainly attributed to the amount of welding applied on the joints and also extreme heats produced in welding process, which could change the mechanical behaviour of the beam.

For the horizontal and vertical-corrugated web types, similar bending mode has been observed for the finite element and experimental tests. However, the flat web beams show a different bending mode at the late stage, where the finite element tests show little web rippling compared to the experimental tests. This is attributed to the definition of the hardening curve. Although there is a difference in the bending mode at the late stage, this would not affect the findings

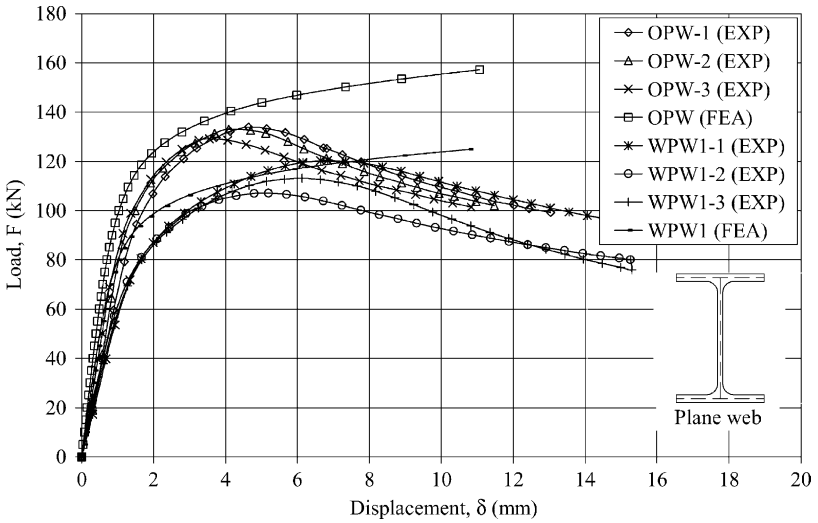

Fig. 15. Comparison of F–δ curves (plane web beams).

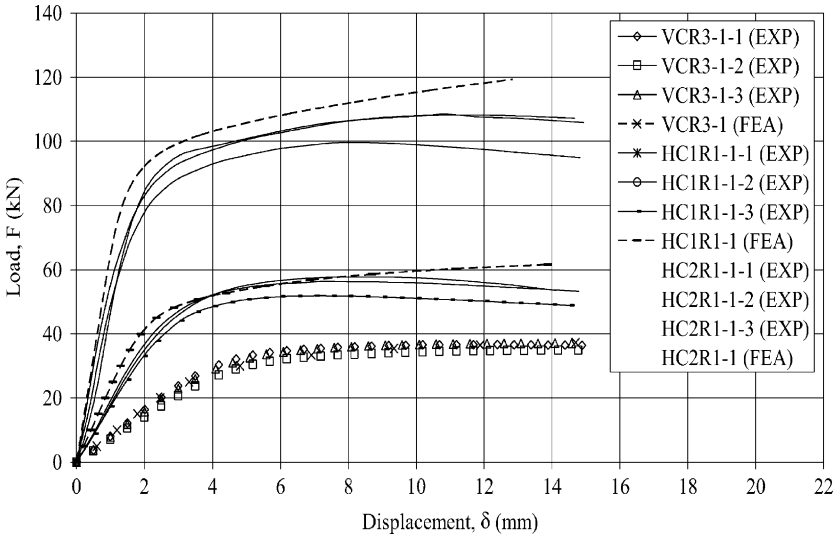

Fig. 16. Comparison of F–δ curves (corrugated web beams).

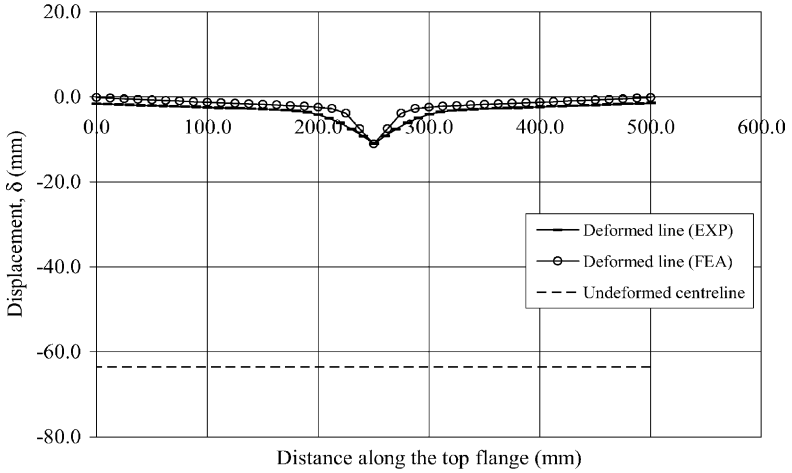

Fig. 17. Comparison of top flange's deformation for OPW model obtained from CMM measurements and finite element analysis.

of this project because concentration was done on the early elastic bending stage.

The comparison charts are shown in Figs. 15 and 16. In addition, the deformed profile was also measured by using the CMM machine and the two-dimensional section plots utility (LUSAS's post-processing tool) as presented in Fig. 17.

8. Conclusions

In this investigation, the bending capacity of structural beams with semicircular corrugated webs in both horizontal and vertical directions has been studied both experimental and computational. A non-linear finite element software (LUSAS) was used for these purposes. The effects of web corrugation to the bending capacity and geometrical parametric studies on variables such as web thickness, corrugation radius and corrugation direction were reported. Comparisons of results were also made between both methods of study to evaluate the accuracy of the developed finite element model. Based on results obtained, the following conclusions are drawn:

1. The beams with vertical-corrugated web could sustain between 13.3 and 32.8% higher load than the geometrical identical plane web beams under three pin point bending, within the range of corrugation radius taken.
2. Web corrugation in the vertical direction (along the length) contributed higher bending capacity than in the horizontal direction (in the cross-section plane). The ratio of yield load for VCR to HC1R is within the range of 1.32–1.89 and in comparison to HC2R, the ratio was 1.56–3.26.
3. The beam's weight could be reduced by 13.6% by using vertically corrugated web with the maximum size of corrugation radius.
4. Higher moment capacity is achieved with larger corrugation radius. The highest increments obtained were 1.68, 2.44 and 1.17 times for HC1R, HC2R and VCR models, respectively.
5. Deformation was initiated at the compression flange in bending mode in the elastic state for all experimental and finite element models, while no occurrence of weld failure was observed.

It is undoubted that the bending capacity of structural beams is further enhanced by using vertical-corrugated web. However, the design of beams with semicircular corrugation profile is limited by the flange's width and cycle length. Thus, the corrugation sizes need to be optimised in order to accommodate wider range of applications and considering the manufacturability of these corrugated web beams. Finally, the influences of variables such as the flange thickness and material properties, cycle length and amplitude, and mode of analysis are areas open for future research.

References

[1] W. Zhang, Y. Li, Q. Zhou, X. Qi, G.E.O. Widera, Optimization of the structure of an H-beam with either a flat or a corrugated web. Part 3. Development and research on H-beams with wholly corrugated webs, J. Mater. Process. Technol. 101 (1) (2000) 119–123.
[2] M. Elgaaly, R.W. Hamilton, A. Seshadri, Shear strength of beams with corrugated webs, J. Struct. Eng. ASCE 122 (4) (1996) 390–398.
[3] M. Elgaaly, A. Seshadri, R.W. Hamilton, Bending strength of steel beams with corrugated webs, J. Struct. Eng. ASCE 123 (6) (1997) 772–782.
[4] M. Elgaaly, A. Seshadri, Girders with corrugated webs under partial compressive edge loading, J. Struct. Eng. ASCE 123 (6) (1997) 783–791.
[5] R.P. Johnson, J. Cafolla, Local flange buckling in plate girders with corrugated webs, in: Proceedings of the Institution of Civil Engineers, Structures and Buildings, vol. 122, No. 2, 1997, pp. 148–156.
[6] R.P. Johnson, J. Cafolla, Corrugated webs in plate girders for bridges, in: Proceedings of the Institution of Civil Engineers, Structures and Buildings, vol. 122, No. 2, 1997, pp. 157–164.
[7] Y. Li, W. Zhang, Q. Zhou, X. Qi, G.E.O. Widera, Buckling strength analysis of the web of a WCW H-beam. Part 2. Development and research on H-beams with wholly corrugated webs (WCW), J. Mater. Process. Technol. 101 (1) (2000) 115–118.